

# Di-neutrons in neutron matter within Brueckner–Hartree–Fock approach

Felipe Isaule,<sup>1</sup> H. F. Arellano,<sup>1,2</sup> and Arnau Rios<sup>3</sup>

<sup>1</sup>*Department of Physics – FCFM, University of Chile,  
Av. Blanco Encalada 2008, Santiago, Chile*

<sup>2</sup>*CEA,DAM,DIF F-91297 Arpajon, France*

<sup>3</sup>*Department of Physics, Faculty of Engineering and Physical Sciences,  
University of Surrey, Guildford, Surrey GU2 7XH, United Kingdom*

(Dated: September 29, 2016)

## Abstract

We investigate the appearance of di-neutron bound states in pure neutron matter within the Brueckner–Hartree–Fock approach at zero temperature. We consider the Argonne  $v_{18}$  and Paris bare interactions as well as chiral two- and three-nucleon forces. Self-consistent single-particle potentials are calculated by controlling explicitly singularities in the  $g$  matrix associated with bound states. Di-neutrons are loosely bound, with binding energies below 1 MeV, but are unambiguously present for Fermi momenta below  $1 \text{ fm}^{-1}$  for all interactions. Within the same framework we are able to calculate and characterize di-neutron bound states, obtaining mean radii as high as  $\sim 110 \text{ fm}$ . Implications of these findings are presented and discussed.

PACS numbers: 21.45.Bc, 21.65.-f, 26.60.Kp, 21.30.Fe, 21.65.Cd

## I. INTRODUCTION

Di-neutrons have been investigated in a variety of regimes and their imprint is recognized in the low-energy behavior of phase shifts in neutron-neutron scattering [1–4]. Bound and resonant states in few-neutron systems have been discussed both in recent experiments [5] and in the theoretical nuclear physics literature [6]. Although the interaction between two neutrons in free space is attractive, its strength is not enough to counterbalance the kinetic contribution of a confined system, as implied by Heisenberg’s uncertainty principle. However, early in the 70s Migdal conjectured the possibility of di-neutrons in the nuclear medium [7], opening the way to copious research on neutron pairing, superfluidity and clustering in nuclear systems [8–11].

The study we present in this work focuses on di-neutron bound-state structures in homogeneous neutron matter in the context of the Brueckner–Hartree–Fock (BHF) approach, when realistic internucleon bare interactions are used. Because of this, it offers the possibility to be solved *ab initio* without additional parameters. A novel element in this study is the accurate account for di-nucleon contributions in the evaluation of single-particle (sp) spectra, as recently reported in Ref. [12] by one of us for the case of symmetric nuclear matter based on the Argonne  $v_{18}$  internucleon bare interaction (AV18). The three major conclusions of that work are: *i.*- Nucleon effective masses can reach up to four times the bare nucleon mass; *ii.*- Large size bound states occur at subsaturation densities; and *iii.*- Two different families of sp solutions are found to satisfy self-consistency at low densities, leading to what is known as coexisting sp spectra.

The work we present here aims at re-assessing these properties in the context of pure neutron matter, i.e. restricting the nucleon–nucleon ( $NN$ ) interaction to unit isospin ( $T = 1$ ). Microscopic studies of di-neutron formation in neutron matter, with many-body methods and based on realistic internucleon interactions, have not been discussed extensively in the past. Di-neutron states, if they appear in specific conditions within a neutron star’s life, could have an impact on its properties. Hence, one would still like to assess to what extent the picture that arises when *in-medium* di-nucleons are taken into account is robust under the use of realistic internucleon bare interactions, i.e. independent of two-nucleon (2N) and three-nucleon (3N) forces. Furthermore, it would also be of interest to know what features of di-nucleon structures occurring in symmetric nuclear matter remain in the limit of pure

neutron matter.

The study of neutron matter properties over a wide range of densities is one of the quests of modern nuclear theory [13]. At low densities, neutron matter may provide important clues for the understanding of neutron-rich nuclei, surface-related nuclear phenomena and clustering [9]. At neutron densities near and above nuclear saturation, superfluid pairing is recognized as a key element to describe the cooling evolution of neutron stars [10]. Additionally, the equation of state (EoS) for nuclear matter plays a central role in the description of hydrostatic equilibrium of neutron stars [14]. With these considerations in mind, we supplement such studies with *ab initio* calculations for *in-medium* di-neutron bound states, which represent the first step towards a full microscopic theory of clustering in dense matter. Our calculations only include two-body clusters, but do so in a theoretically consistent way that does not require phenomenological parameters [15]. In particular, our results could provide input for the more sophisticated cluster models that are employed in astrophysical simulations [9, 15, 16].

The appearance of two-body bound states in dense, correlated media is key problem of interest to quantum many-body theory. The competition, or crossover, between dimers and Cooper pairs has been discussed extensively in the cold atom community [17]. In neutron matter, a crossover of the same type is also expected to appear [18–21]. While a detailed discussion of the crossover goes beyond the scope of our preliminary analysis, we point out some similarities between the di-neutron bound states and Cooper pairs, which point at a subtle relation between the two [22–24].

This article is organized as follows. In Sec. II, we lay out the theoretical framework under which di-nucleons shall be investigated. In Sec. III, we present results for sp spectra in the case of neutron matter using realistic  $NN$  potentials. Furthermore, we examine the occurrence of di-neutrons, their spatial properties and effective masses. We also provide a comparison of di-neutron bound states with Cooper pairs and superfluid solutions in pure neutron matter. As an application of our findings we also investigate the EoS of neutron matter. Finally, we present a summary and conclusions of the work in Sec. IV .

## II. FRAMEWORK

The BHF approach for interacting nucleons in nuclear matter can be identified as the lowest-order approximation of Brueckner–Bethe–Goldstone theory or self-consistent Green’s function theory at zero temperature [25]. In either case, in the context of homogeneous nuclear matter, the effective interaction is described by a  $G$  matrix, an operator that depends on the density of the medium, and a starting energy  $\omega$ . When only 2N correlations are taken into account in the ladder approximation, the  $G$  matrix satisfies

$$G(\omega) = v + v \sum_{\mathbf{k}_a, \mathbf{k}_b} |\mathbf{k}_a \mathbf{k}_b\rangle \times \frac{[1 - n(k_a)][1 - n(k_b)]}{\omega + i\eta - e(k_a) - e(k_b)} \langle \mathbf{k}_a \mathbf{k}_b | G(\omega), \quad (1)$$

where  $v$  corresponds to the bare interaction between nucleons;  $e(k) \equiv e_k$ , is the sp energy given in terms of the sp potential,  $U(k)$ ,

$$e_k = \frac{k^2}{2m} + U(k); \quad (2)$$

and  $n(k)$  corresponds to the momentum distribution. The density is obtained from the latter through the relation

$$\rho = \nu \sum_{\mathbf{k}} n(k), \quad (3)$$

where  $\nu = 2(4)$ , for neutron (nuclear) matter. At zero temperature, the momentum distribution is a step function,  $n(k) = \Theta(k_F - k)$ , with  $k_F$  being the Fermi momentum,

$$\rho = \nu \frac{k_F^3}{6\pi^2}. \quad (4)$$

The  $G$ -matrix in Eq. (1) enables the evaluation of the sp potential,

$$U(k) = \text{Re} \sum_{\mathbf{p}} n(p) \langle \frac{\mathbf{k}-\mathbf{p}}{2} | g_{|\mathbf{k}+\mathbf{p}|} (e_k + e_p) | \frac{\mathbf{k}-\mathbf{p}}{2} \rangle_A, \quad (5)$$

where  $g_K(\omega)$  represents the reduced  $G(\omega)$  matrix for total pair momentum  $\vec{K} = \vec{k} + \vec{p}$ , after a momentum-conserving Dirac  $\delta$  function has been factored out. The subscript  $A$  denotes the antisymmetrization of the ket state. Self-consistency of Eqs. (1), (2) and (5) is achieved iteratively. We use of the continuous choice for the sp spectrum, where the condition expressed by Eq. (5) is imposed on all momenta  $k$ . This choice of sp potential yields better convergence in terms of the hole-line expansion [26].

In the iterative procedure to determine  $U(k)$ , actual bound states appear while evaluating Fermi-motion integrals in Eq. (5). As found in symmetric nuclear matter, the appearance of bound states is more relevant at subsaturation densities [12], where di-nucleon singularities take place in both the  $^1S_0$  and  $^3SD_1$  channels. This feature has resulted in the identification of two distinct families of sp solutions meeting self-consistency: Phase I, for  $0 \leq k_F \lesssim 0.29 \text{ fm}^{-1}$ ; and Phase II, for  $k_F \gtrsim 0.13 \text{ fm}^{-1}$ . Over the range  $0.13 \lesssim k_F \lesssim 0.29 \text{ fm}^{-1}$ , the two families satisfy self-consistency criteria, and are referred to as “coexisting solutions” in Ref. [12]. The scenario for pure neutron matter is different, since the isoscalar channel is suppressed, ruling out contributions to the sp potential from the  $^3SD_1$  state. As a result, we find that pure neutron matter does not allow for coexisting sp spectra.

An appealing feature of the BHF approach is that it enables a direct link between the bare interaction among constituents and properties of interacting nucleons in a homogeneous environment. Microscopic, phase-shift equivalent nuclear interactions predict different *in-medium* properties [27]. In this work, we explore a variety of nuclear interactions in an effort to provide robust predictions for di-neutron properties. We use the traditional Argonne  $v_{18}$  [28] and Paris [29] bare potentials, which have been fit to  $NN$  phase-shift data at beam energies below pion production threshold, together with static properties of the deuteron. Additionally, we also include a chiral effective-field-theory ( $\chi$ EFT) interaction, which is based on chiral perturbation theory. The resulting bare interaction is constructed with nucleons and pions as degrees of freedom, with the 2N part fit to two-nucleon data. We consider the chiral 2N force (2NF) up to next-to-next-to-next-to-leading order ( $N^3\text{LO}$ ) given by Entem and Machleidt [30]. In addition, we also consider chiral 3N forces (3NF) in  $N^2\text{LO}$ , using a density-dependent 2NF at the two-body level [31, 32]. This density-dependent contribution does not contain correlation effects [33], and is added to the bare 2NF in the calculation of the  $G$ -matrix. The corresponding Hartree-Fock contribution is subtracted at each iteration to avoid any double counting. For this chiral 3NF contribution, we use the low energy constants  $c_D = -1.11$  and  $c_E = -0.66$ , reported in Ref. [34], which describe the  $^3\text{H}$  and  $^4\text{He}$  binding energies with unevaluated  $NN$  interactions. We also note that we have used a chiral cutoff of  $\Lambda_\chi = 700 \text{ MeV}$ . Because the main aim of our work is not the estimation of systematic effects, we do not explore the cutoff or low-energy-constant dependence of our results. Instead, we will focus most of our analysis on the region where all predictions for di-neutron bound states are robust (or invariant with respect to the

underlying potential). Roughly speaking, we find that results with different interactions are equivalent below  $k_F = 1.5 \text{ fm}^{-1}$ .

### III. RESULTS

We have obtained self-consistent solutions for  $sp$  potentials for pure neutron matter in the BHF approximation within the continuous choice following the techniques described in Ref. [12]. Calculations were made by considering all partial waves up to  $J = 7$  in the total angular momentum, regardless of the density. Di-nucleon occurrences in the  $^1S_0$  and  $^3P_F$   $NN$  channels are explicitly treated. Files containing self-consistent  $sp$  potentials discussed in this work can be retrieved from Ref. [35].

#### A. Solutions

In Fig. 1, we show self-consistent solutions  $U(k)$  for pure neutron matter as a function of  $sp$  momentum,  $k$ . We include results corresponding to AV18 (short-dashed curves), Paris (dash-dotted curves), N3LO<sub>2N</sub> (dashed curves) and N3LO<sub>2N</sub>+N2LO<sub>3N</sub> (solid curves). Figures 1(a)-1(d) represent solutions for  $k_F = 1.0, 1.4, 1.6$ , and  $1.8 \text{ fm}^{-1}$ , respectively. These Fermi momenta correspond to neutron densities between  $0.03$  and  $0.2 \text{ fm}^{-3}$ , with the latter close to the saturation density of symmetric nuclear matter. Dashed vertical lines in each panel represent the corresponding Fermi momentum. We keep the same vertical scale throughout for clarity. The results shown in Fig. 1(a) for  $k_F = 1 \text{ fm}^{-1}$  provide evidence for nearly identical behavior for all four interactions for  $k < 3.5 \text{ fm}^{-1}$ . This similarity points to a dominance of many-body correlations in the low density regime, so that individual  $NN$  force features are not explicitly resolved.

In Figs. 1(c) and 1(d), where  $k_F \geq 1.6 \text{ fm}^{-1}$ , we identify two aspects of interest. On the one hand, for momenta below about  $k \lesssim 2 \text{ fm}^{-1}$ , the  $sp$  solutions based on N3LO<sub>2N</sub> follow the trend given by AV18 and Paris interactions. The “low-momentum” part of  $U(k)$  becomes more and more attractive with density, and is mildly dependent on momentum up to the corresponding  $k_F$ . As long as 2NF are used, this low-momentum components are relatively independent of the nuclear interaction. In contrast, the  $sp$  solution based on the N3LO<sub>2N</sub>+N2LO<sub>3N</sub> interaction is substantially more repulsive at low momenta. This agrees

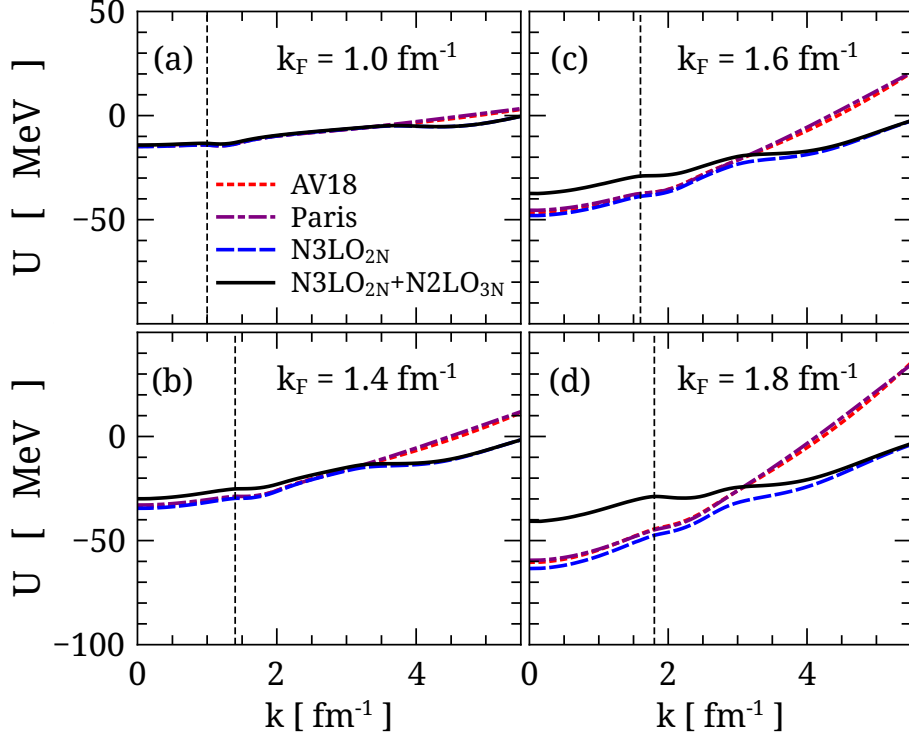


FIG. 1. BHF self-consistent sp potentials for pure neutron matter as a functions of sp momentum,  $k$ . Short-dashed, dash-dotted, dashed and solid curves correspond to AV18, Paris,  $N3LO_{2N}$  and  $N3LO_{2N}+N2LO_{3N}$  bare potentials, respectively. Panels (a)-(d) present solutions for  $k_F = 1.0, 1.4, 1.6$ , and  $1.8 \text{ fm}^{-1}$ , respectively.

with the intuitive idea that 3NF provide repulsion in the  $T = 1$  channel [32]. We note in particular that the low-momentum part of  $U(k)$  becomes more and more repulsive as the density increases when 3NF are considered.

On the other hand, for  $k \gtrsim 3 \text{ fm}^{-1}$  the sp solutions for the two chiral interactions get closer to each other as momentum increases, departing markedly from the trend based on AV18 and Paris potentials. Whereas traditional interactions have strong short-range cores, chiral forces are cut off by construction. As a consequence, there is no support in the bare interaction for any high-momentum components of  $U(k)$ . In particular, one can see that a sharp relative momentum cutoff at  $\Lambda$  will affect sp spectra at sp momenta  $k > 2\Lambda - k_F$ . The Entem-Machleidt interaction has  $\Lambda = 500 \text{ MeV}$  ( $\sim 2.5 \text{ fm}^{-1}$ ), and hence the similarity between the two forces beyond about  $3 \text{ fm}^{-1}$  can be ascribed to the disappearance of the matrix elements at high momenta. In contrast, “hard core” forces like Paris and AV18

still have active components at large  $k$ , giving rise to nonzero spectra at arbitrarily large momenta.

The study of neutron effective masses  $m^*$  in both low- and high-density neutron matter has been a subject of increasing interest over the past few years [36, 37]. The calculated sp spectra of Eq. (2) provide access to the effective mass,

$$\frac{m^*}{m} = \frac{k_F}{m} \left[ \frac{\partial e_k}{\partial k} \right]_{k=k_F}^{-1}, \quad (6)$$

where  $m$  stands for nucleon bare mass. We show in Fig. 2 the calculated effective-to-bare mass ratio  $m^*/m$  as a function of Fermi momentum for the four interactions discussed above. Figures 2(a)-2(d) correspond to results based on AV18, Paris, N3LO, and N3LO<sub>2N</sub>+N2LO<sub>3N</sub>, respectively. We focus our discussion around two basic issues. First, the ratio  $m^*/m$  for the four interactions follows almost identical behaviors for Fermi momenta below  $1.5 \text{ fm}^{-1}$ . We take this as an indication of the robustness of our results. Starting, as expected, from a value of  $m^* = m$  at low density, the effective mass grows with  $k_F$  and reaches a maximum of around  $\sim 1.2m$  at Fermi momenta in the range  $0.3 - 0.4 \text{ fm}^{-1}$ . From this point on, the effective mass decreases and becomes smaller than  $m$  above  $k_F \approx 1 \text{ fm}^{-1}$ . As we shall discuss in the following, the density regime where  $m^* > m$  is nearly the same as that where di-neutron bound states take place. Furthermore, in the context of the sp potentials of Fig. 1, we emphasize that  $m^* > m$  states will be found whenever the sp potential is a decreasing function of momentum around  $k_F$ . This is indeed the case in Figs. 1(a) and 1(b), where one can identify a wiggly structure around  $k_F$ . We note that effective masses at such low densities are relevant for the physics of neutron star crusts, which plays an important role in the description of pulsar glitches by entrainment effects [36, 38].

Second, we find that effective masses based on 2NF-only calculations tend to decrease with  $k_F$  above the Fermi momentum of  $1.5 \text{ fm}^{-1}$ . In contrast, the ratio  $m^*/m$  for N3LO<sub>2N</sub>+N2LO<sub>3N</sub> starts to grow in this region, while the other three cases decrease monotonically. As a matter of fact, we find a region where  $m^*/m > 1$  for  $k_F$  above  $1.8 \text{ fm}^{-1}$ . Differences in the effective masses between chiral 2NF and 2NF+3NF calculations for  $k_F > 1.5 \text{ fm}^{-1}$  have already been reported in Ref. [32]. As mentioned earlier, values of  $m^*/m$  above 1 indicate the presence of decreasing sp potentials as a function of  $k$ . Figure 1(d) illustrates the appearance of such a structure for the N3LO<sub>2N</sub>+N2LO<sub>3N</sub> calculations. We attribute this decrease to the competition between the strong repulsion induced by 3NF



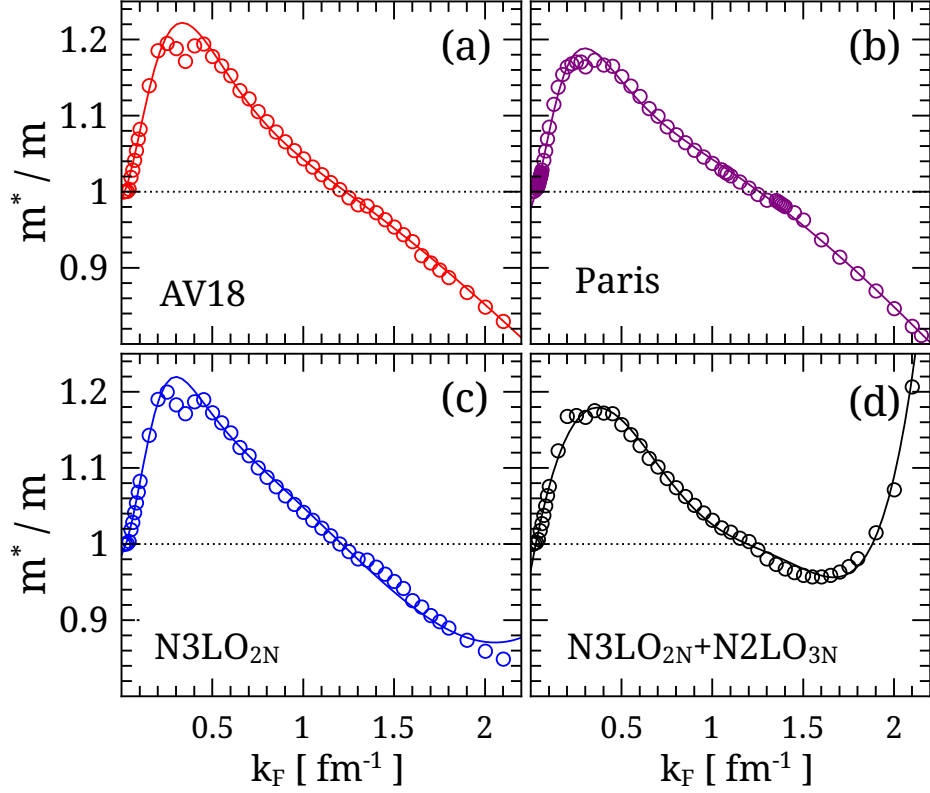


FIG. 2. Effective-to-bare-mass ratio  $m^*/m$  in pure neutron matter as a function of Fermi momentum,  $k_F$ . Panels (a)-(d) correspond to results for AV18, Paris,  $N3LO_{2N}$ , and  $N3LO_{2N}+N2LO_{3N}$  bare potentials, respectively. Continuous curves represent fits based on Eq. (7).

at low momenta and the onset of cutoff effects at momenta close to  $\sim 3 \text{ fm}^{-1}$ . A detailed analysis of this behavior goes beyond the scope of this work, because it would require a study of the low-energy-constant and cutoff dependence of these results.

We found a suitable parametrization for the calculated effective masses in the form

$$\frac{m^*}{m} = 1 + (a_0 + a_2 x^2)P(x) + (b_0 + b_2 x^2 + b_4 x^4)Q(x), \quad (7)$$

where  $x = k_F/b$ , with  $b = 0.2 \text{ fm}^{-1}$  representing a typical Fermi momentum for the effective mass maximum. The functions  $P$  and  $Q$  satisfy  $P + Q = 1$ , with

$$P(x) = \frac{1}{2} \left[ 1 - \tanh \left( \frac{x - x_c}{d} \right) \right], \quad (8)$$

which provides an effective separation for two regions of density dependence. The resulting coefficients for each interaction are summarized in Table I. The continuous curves in Fig. 2 show the resulting  $m^*/m$  parametrizations.

	AV18	Paris	N3LO <sub>2N</sub>	N3LO <sub>2N</sub> +N2LO <sub>3N</sub>
$x_c$	0	0	0.6197	5.390
$d$	1.411	1.186	0.9544	4.193
$a_0$	$-1.158 \times 10^{-1}$	$-1.549 \times 10^{-1}$	$-6.633 \times 10^{-2}$	$-6.313 \times 10^{-1}$
$a_2$	$6.299 \times 10^{-1}$	$6.245 \times 10^{-1}$	$2.905 \times 10^{-1}$	$-1.542 \times 10^{-1}$
$b_0$	$9.668 \times 10^{-2}$	$1.104 \times 10^{-1}$	$1.744 \times 10^{-1}$	$7.771 \times 10^{-1}$
$b_2$	$-2.762 \times 10^{-3}$	$-2.927 \times 10^{-3}$	$-5.751 \times 10^{-3}$	$-1.036 \times 10^{-1}$
$b_4$	$3.128 \times 10^{-6}$	$3.111 \times 10^{-6}$	$2.722 \times 10^{-5}$	$4.467 \times 10^{-4}$

TABLE I. Fit coefficients for the effective mass,  $m^*/m$ , following Eq. (7). Fits were carried out in the range  $0.05 \leq k_F \leq 3 \text{ fm}^{-1}$  for all forces, except for N3LO<sub>2N</sub>+N2LO<sub>3N</sub>, where  $0.05 \leq k_F \leq 2.2 \text{ fm}^{-1}$ .

## B. Di-neutrons in pure neutron matter

Di-neutrons constitute bound states of two neutrons. As such, they have an associated wave function of finite range and eigenenergy below the Fermi surface. Such states do not occur in free space, despite the attractive nature of the interaction as indicated by the  $^1S_0$  scattering length. In the context of BHF equations, the starting energy  $\omega$  at which these states occur satisfies the criterion

$$\det[1 - v\Lambda_K(\omega)] = 0 , \quad (9)$$

with  $\Lambda_K(\omega)$  the particle-particle propagator in Eq. (1) for pairs with total momentum  $K$ . States are only bound below a corresponding *in-medium* threshold, which depends on the sp energies at each iteration. In particular, bound states require that  $\omega < \omega_{th}$ , with  $\omega_{th}$  being the threshold (lowest) sp energy of the pair allowed by Pauli blocking. In the particular case of pairs with their center of mass (c.m.) at rest ( $K = 0$ ), the energy threshold occurs at  $\omega_{th} = 2e(k_F)$ . We search automatically for di-neutrons during the iterative BHF solving process.

Solutions of Eq. (9) lead to a di-neutron binding energy  $b_{nn}$  defined with respect to the corresponding threshold,

$$b_{nn} = \omega - \omega_{th} . \quad (10)$$

Under this convention of sign, also adopted in Refs. [39–41], a bound state has negative energy. In Fig. 3 we show the di-neutron binding energy as a function of Fermi momentum. These results correspond to static bound pairs, where  $K = 0$ . Circles, asterisks, diamonds, and squares represent AV18, Paris, N3LO<sub>2N</sub> and N3LO<sub>2N</sub>+N2LO<sub>3N</sub> interactions, respectively. One of the major conclusions of our work is that all four interactions considered hold bound di-neutrons states at Fermi momenta in the range  $0.05 - 1.05 \text{ fm}^{-1}$ . Di-neutrons are relatively loosely bound, with binding energies below 700 keV. In all cases, the deepest binding takes place at  $k_F \approx 0.6 \text{ fm}^{-1}$ , with binding energies ranging between 550 and 700 keV. AV18 yields the largest binding,  $b_{nn} = -0.7 \text{ MeV}$ , whereas Paris and the chiral interactions produce slightly less bound di-neutrons,  $b_{nn} \approx -0.6 \text{ MeV}$ . Let us emphasize the fact that the prediction of the appearance of di-neutron bound states is extremely robust, in the sense that it is to a large extent independent of the interaction under consideration. We note, in particular, that both the binding energy and the density dependence of the di-neutron states are predicted to be very similar. This is a strong indication that the appearance of di-neutrons is governed by many-body correlations.

The BHF approach offers the appealing possibility of obtaining di-nucleon bound states even beyond the static case. When  $K \neq 0$ , the c.m. of the pair moves relative to the nuclear medium, and thus one expects the binding to decrease as  $K$  increases. We provide an illustrative example of this behavior in Fig. 4, where we show a surface plot for  $b_{nn}/E_d^1$  as a function of  $k_F$  and  $K$ . The bare interaction considered in this case is N3LO<sub>2N</sub>+N2LO<sub>3N</sub>, but a similar behavior is found for the other three interactions. In this case the strongest binding ( $\sim 630 \text{ keV}$ ) occurs for static pairs ( $K = 0$ ) at  $k_F \approx 0.6 \text{ fm}^{-1}$ . As the c.m. momentum increases, binding diminishes smoothly. At  $k_F \approx 0.4 - 0.5 \text{ fm}^{-1}$  di-neutrons take place over a larger range of total momenta, allowing bound states up to  $K$  slightly below  $\sim 0.1 \text{ fm}^{-1}$ . This bodes well with the idea that di-neutrons can propagate more easily in a relatively dilute and uncorrelated medium, before they are affected by Pauli blocking at large densities. Note that for  $k_F \rightarrow 0$ , di-neutrons get dissolved, as should be expected from realistic interactions that do not hold bound states in free space in the channel  $^1S_0$ . This feature contrasts with the deuteron channel in symmetric nuclear matter, where a binding energy of -2.22 MeV is allowed for all  $K \geq 0$  in the case  $k_F = 0$ . On the other hand, as  $k_F$  increases, di-neutrons get dissolved. As we shall discuss in the following sub-section, this feature appears related

---

<sup>1</sup> Here,  $E_d$  corresponds to the binding energy of the deuteron in free space.

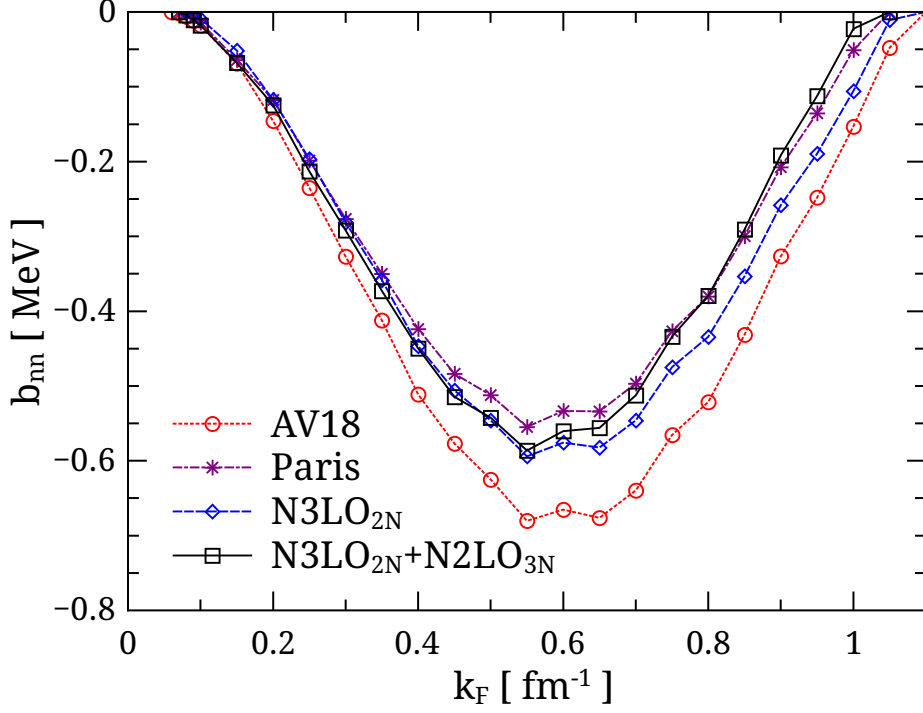


FIG. 3. Di-neutron binding energy in pure neutron matter as a function of Fermi momentum. Circles, asterisks, diamonds and squares correspond to AV18, Paris,  $N3LO_{2N}$  and  $N3LO_{2N}+N2LO_{3N}$  bare potentials, respectively. Results correspond to pairs with zero total momentum.

to the fact that the effective mass gets close to or smaller than the neutron bare mass.

### C. Bound state wave functions

As we have just discussed, singularities of  $g_K(\omega)$  in the  $^1S_0$  and  $^3PF_2$  channels on the real energy axis at energies below the threshold (i.e.  $\omega < \omega_{th}$ ) point to di-neutron bound states. In the following, we discuss the procedures that we have followed to obtain the associated *in-medium* bound-state wave functions. Let  $\omega_{nn}$  be the eigenenergy corresponding to one such bound state. One can show that, for starting energies close to the real axis, the  $G$ -matrix fulfills the equation [12]

$$\lim_{\eta \rightarrow 0} i\eta g_K(\omega_{nn} + i\eta) = vQ|\psi\rangle\langle\psi|Qv, \quad (11)$$

with  $Q$  being the Pauli blocking operator and  $|\psi\rangle$  being the corresponding eigenstate. On the other hand, consider the wave equation for  $|\psi\rangle$  associated with Eq. (1),

$$(\omega_{nn} - \hat{e}_1 - \hat{e}_2)|\psi\rangle = QvQ|\psi\rangle,$$

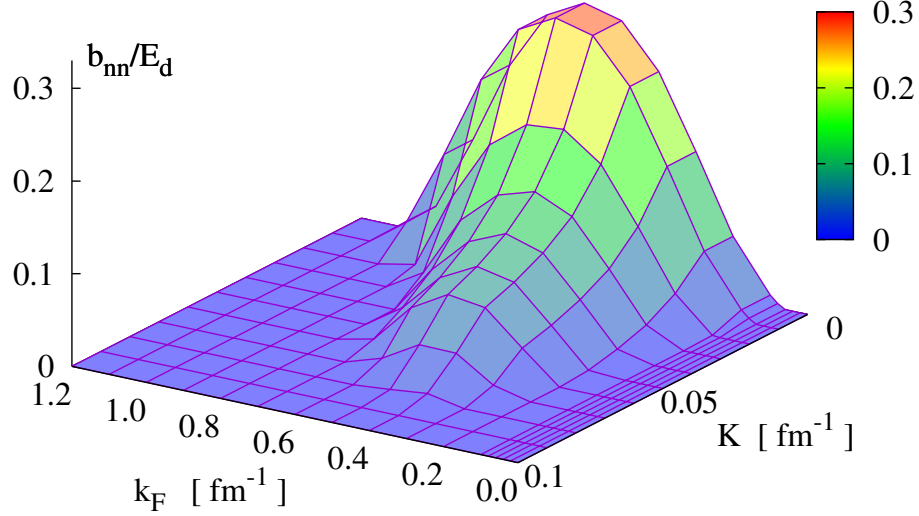


FIG. 4. Di-neutron binding energy, relative to the deuteron binding energy in vacuum, as a function of the pair momentum  $K$  and  $k_F$  in pure neutron matter. Results have been obtained with the N3LO<sub>2N</sub>+N2LO<sub>3N</sub> interactions.

from which we obtain the projected wave function in momentum space,

$$\psi(q) = \frac{\langle q|QvQ|\psi\rangle}{\omega_{nn} - E_K(q)}. \quad (12)$$

Here,  $E_K(q) = \langle e(k_a) + e(k_b) \rangle$ , corresponds to the angle-averaged particle-particle energy when  $\mathbf{k}_{a,b} = \mathbf{K} \pm \frac{1}{2}\mathbf{q}$ . In the case of pairs without c.m. motion relative to the nuclear medium, the numerator reduces to  $\Theta(q - k_F)\langle q|vQ|\psi\rangle$ , indicating that di-nucleon wave functions in the nuclear medium cannot contain momentum components that are already occupied by single particles.

The wave function  $\Psi(q)$  can be obtained after  $\langle q|vQ|\psi\rangle$  is extracted from Eq. (11). We achieve this numerically after solving  $g_K(\omega_{nn} + i\eta)$  for a series of small values of  $\eta$  and extrapolating  $\eta \rightarrow 0$  afterwards. In the case of uncoupled channels with orbital angular momentum  $L$ , the wave function in coordinate space is obtained from the usual Bessel transform

$$\Psi(r) = \sqrt{\frac{2}{\pi}} \int_{\bar{q}}^{\infty} q^2 dq j_L(qr) \psi(q). \quad (13)$$

We note, however, that there is a lower integration bound,  $\bar{q}$  that corresponds to that allowed by Pauli blocking.

In Fig. 5, we show the radial probability density  $r^2|\Psi(r)|^2$  for *in-medium* di-neutrons in the  $^1S_0$  channel at  $k_F = 0.6 \text{ fm}^{-1}$ . Short-dashed, dash-dotted, dashed and solid curves represent solutions corresponding to AV18, Paris, N3LO<sub>2N</sub> and N3LO<sub>2N</sub>+N2LO<sub>3N</sub> solutions, respectively. The spatial distribution of di-neutrons is very similar for the four potentials considered, with small deviations only in the innermost region. A clear, long-range oscillatory pattern is found, as expected from a Pauli-blocked state in the medium. The nodes of the oscillations occur with a periodicity near 5.2 fm, and the overall spatial structure is reminiscent of a Cooper-pair wave function when  $\Psi(r) \sim \cos(k_F r)/r$  [42, 43]. As we see in the following subsection, the oscillatory behavior will give rise to large mean radii, a trend which has also been observed for  $^1S_0$  bound states in symmetric nuclear matter [12]. For reference purposes, we include in this plot the corresponding deuteron wave function in free space (gray-filled curve). Whereas the di-neutron wave-function is modulated by oscillatory medium effects and extends to large relative distances, the corresponding deuteron wave function is confined to within a few fm of the origin. The maximum of the deuteron density occurs slightly below the first peak of the di-neutron wave function, but the overall structure of the two wave functions in that region is similar.

Mean radii,  $\langle r \rangle$ , which are associated with the loosely bound di-neutrons, can be very large. In Fig. 6 we plot  $\langle r \rangle$  as a function of Fermi momentum for the four interactions under consideration. These radii were obtained by resorting to Laplace transforms, as described in Ref. [12]. The values of these mean radii are extremely large, above 60 fm in all cases. Their density dependence follows closely that of the binding energies in Fig. 4. The more a di-neutron state gets bound, the more compact it becomes. In accordance, mean radii increase substantially in the regions where di-neutrons get diluted, and we find values of mean radii exceeding 110 fm.

In keeping with the robustness of the bound-state energies, the mean radii are remarkably insensitive to the underlying nuclear interaction. The behavior of  $\langle r \rangle$  for both chiral interactions are very similar, pointing to a weak influence of 3NF on low-density, weakly bound di-neutron bound states. When comparing these two potentials with AV18, the latter yields more compact di-neutrons, by about 10 fm. This is to be expected in view of the slightly more attractive energies found in Fig. 3. Overall, however, the density dependence

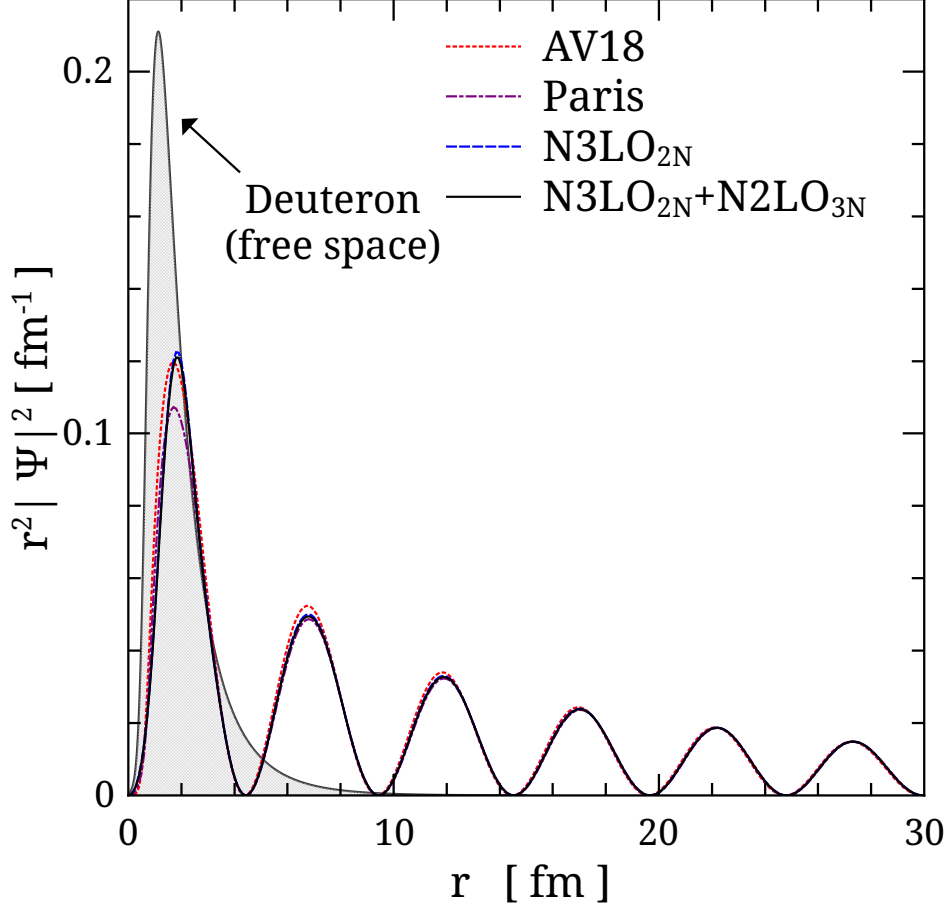


FIG. 5. Radial probability density,  $r^2|\Psi(r)|^2$ , for di-neutron bound states in pure neutron matter ( $k_F = 0.6 \text{ fm}^{-1}$ ) as a function of the relative distance. Short-dashed, dash-dotted, dashed and solid curves correspond to AV18, Paris,  $\text{N3LO}_{2N}$  and  $\text{N3LO}_{2N}+\text{N2LO}_{3N}$  bare potentials, respectively. Gray filled curve represents the deuteron (S- and D-waves) probability density in free space based on the AV18 bare potential.

and absolute value of  $\langle r \rangle$  seems to be purely determined by many-body correlations.

As discussed in Ref. [12], effective masses greater than the bare mass favor the formation of a bound state if a weakly attractive interaction is active. To explore this point in the context of pure neutron matter, we investigate the occurrence of di-neutrons in the  $^1S_0$  channel by suppressing the sp potential, while considering the nucleon mass equal to the effective mass at the Fermi surface, that is  $e_k \rightarrow k^2/2m^*$ , with  $m^*$  obtained from Eq. (6). The effective mass approximation is only employed in the search for di-neutrons, but not in self-consistent BHF calculation. Indeed, if the effective mass is the main driver for the formation of bound

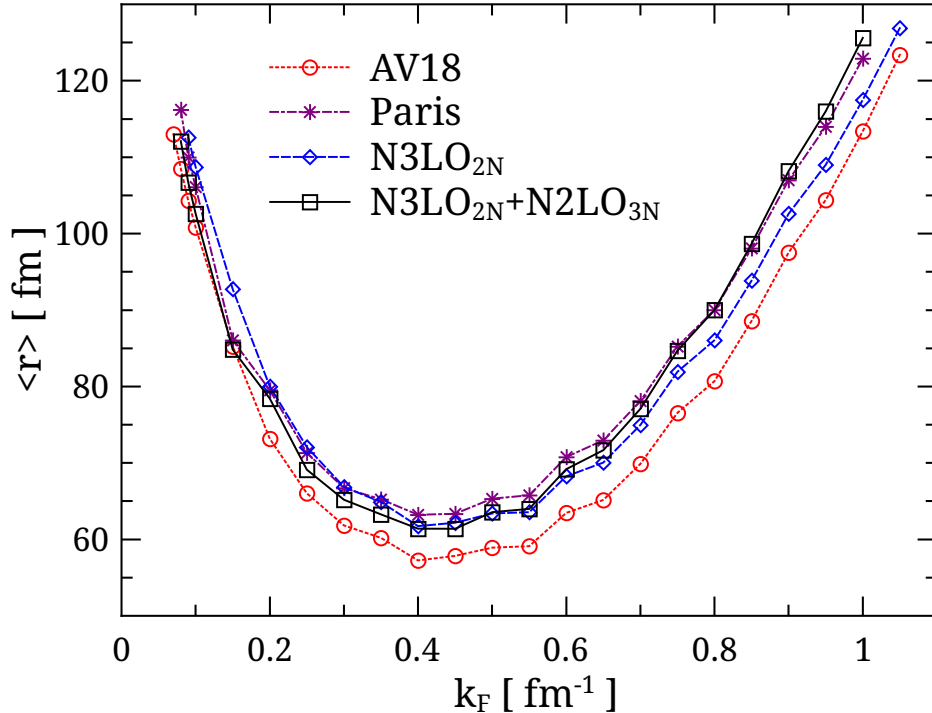


FIG. 6. Mean radius  $\langle r \rangle$  for di-neutrons in pure neutron matter as a function of  $k_F$ . Circles, asterisks, diamonds and squares correspond to AV18, Paris, N3LO<sub>2N</sub> and N3LO<sub>2N</sub>+N2LO<sub>3N</sub> bare potentials, respectively.

states, the results should be insensitive to the removal of the detailed momentum dependence when the spectrum is replaced by the constant  $m^*$ . In Figs. 7(a) and 7(b) we plot di-neutron binding energies,  $b_{nn}$  (a), and mean radii  $\langle r \rangle$ , respectively, following the strategy described above. Solid curves denote results based on  $e_k = k^2/2m^*$ , with  $m^*$  taken from the parametrization given in Eq. (7). We compare these results to the exact calculations (filled circles). We observe that the range in  $k_F$  where  $b_{nn} \neq 0$  is nearly the same in both cases, and it also coincides with the region in Fig. 2 where  $m^*/m > 1$ . Moreover, the exact and the approximate calculations yield qualitatively and quantitatively similar binding energies and mean radii. Overall, this supports our interpretation connecting bound-state formation and relatively large effective masses. In this respect, effective masses greater than bare masses seem to favor a binding mechanism for interacting neutrons.

In terms of quantitative differences, the effective mass approximation produces slightly less bound di-neutron states, but reproduces the overall density dependence of the full calculations. In terms of radii, we find again that the shallowest bound states, occurring at



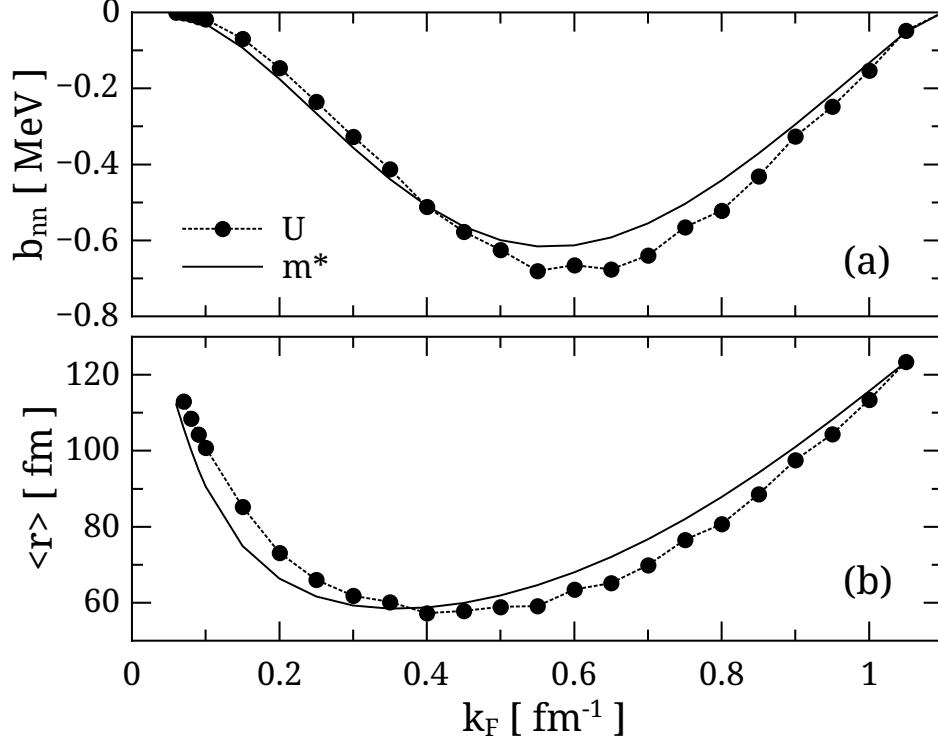


FIG. 7. (a) Di-neutron binding energy and (b) mean radii as a function of Fermi momentum,  $k_F$ , for two choices of sp spectrum. Dashed curves with filled circles are obtained by considering the full spectrum,  $e(k) = k^2/2m + U(k)$ , whereas solid curves are obtained with the approximation  $e(k) = k^2/2m^*$ , with  $m^*$  obtained from Eq. (6). Results are based on the AV18 bare interaction, but similar results are obtained with other interactions.

$k_F \sim 0.06$  and  $1.05 \text{ fm}^{-1}$ , are those which yield the most spread density distributions. We notice, however, that an effective-mass approximation for the sp spectrum based on exact effective masses yields quantitatively different mean radii and binding energies (as functions of density) relative to the exact sp solutions. The most compact di-neutron appears at  $k_F \approx 0.3 \text{ fm}^{-1}$ , slightly below the exact calculations, although the overall radius values are very similar. While we do not show more results here, we note that similar results are obtained with other  $NN$  interactions.

#### D. Contact with Cooper pairs and di-neutron condensate

As described in previous sections, *in-medium* di-neutrons of total pair momentum  $K$  are identified as poles of  $g_K(\omega)$  at energies below the Fermi surface. The corresponding wave functions represent confined, although extended, probability distributions for the bound pairs. For vanishing total momentum, these solutions have a close correspondence to Cooper pairs in interacting Fermi systems, and the subsequent emergence of superfluid states. To sustain this remark we have solved Cooper's equation [44] given by

$$(2e_k - \omega)\psi(k) = -\frac{2}{\pi} \int_{k_F}^{\infty} k'^2 dk' v(k, k') \psi(k') , \quad (14)$$

where  $v$  represents the bare potential, and  $e_k$  the sp energy. After discretization, this equation can be reduced to a matrix equation to obtain its eigenenergy  $\omega$  and corresponding eigenfunction  $\psi(k)$  of a Cooper pair. The condensation of Cooper pairs in fermionic systems can be described in BCS theory, where the energy gap  $\Delta(k)$  for an uncoupled  $NN$  state satisfies

$$\Delta_k = -\frac{2}{\pi} \int_0^{\infty} k'^2 dk' v(k, k') \frac{\Delta_{k'}}{2E_{k'}} . \quad (15)$$

Here  $E_k = \sqrt{(e_k - \mu)^2 + \Delta_k^2}$ , represents a quasiparticle energy, with  $\mu$  being the chemical potential. The normal and anomalous density distributions corresponding to this collective condensed many-body state are given by

$$n(k) = \frac{1}{2} \left( 1 - \frac{e_k - \mu}{E_k} \right) , \quad (16)$$

$$\kappa(k) = \frac{\Delta_k}{2E_k} , \quad (17)$$

respectively. The chemical potential is obtained from the condition

$$\rho = 2 \int \frac{d^3k}{(2\pi)^3} n(k) , \quad (18)$$

with  $\rho = k_F^3/3\pi^2$  being the neutron density. Solutions to the gap equation, involving Eqs. (15), (16) and (18), can be obtained following the method introduced by Baldo *et al.* [45].

Equation (15) for the energy gap can be recast in terms of the anomalous density defined by Eq. (17),

$$2\sqrt{(e_k - \mu)^2 + \Delta_k^2} \kappa(k) = -\frac{2}{\pi} \int_0^{\infty} k'^2 dk' v(k, k') \kappa(k') . \quad (19)$$

Note that if  $|\Delta_k| \ll |e_k - \mu|$ , then Eq. (19) for the anomalous density becomes similar to Eq. (14), where we identify  $\omega = 2\mu$ . An important difference between these two equations is the fact that the anomalous density is nonzero below the Fermi surface, in contrast with BHF di-neutrons and Cooper pairs at zero temperature whose wave functions have fully suppressed their momentum components below the Fermi surface. The implication of this difference is on the range of the density distributions.

In Fig. 8 we plot the radial probability density for di-neutrons in the  $^1S_0$  channel obtained from the BHF equation (solid curves), Cooper-pair wave equation (long-dashed curves) and BCS anomalous density (short-dashed curves). For comparison we include in all frames the  $^3S_1$ -channel deuteron radial probability density in free space, represented with red-shaded curves. Figures 8(a)-8(c) correspond to solutions for  $k_F = 0.25, 0.60$ , and  $1.0 \text{ fm}^{-1}$ , respectively. We observe that BHF di-neutron and Cooper pair density distributions are very similar to each other, exhibiting long-range behavior with oscillatory pattern with periodicity  $\Delta r = \pi/k_F$ . The anomalous density distribution also shows an oscillatory pattern, although more confined than in the case of Cooper pairs. This difference in size stems from the fact that Cooper pairs and BHF di-neutrons have a cutoff of momenta below the Fermi surface, which is a feature that the condensate distribution does not have. In all cases, the sizes of di-neutrons, Cooper pairs and anomalous density appear considerably more extended than the deuteron in free space. It is important to note at this point that Cooper pairs and di-neutrons in BHF correspond to the same object. In this context, self-consistent potentials reported here account explicitly for Cooper pairs as described in Ref. [12].

### E. Equation of State

In addition to its intrinsic theoretical value in the study of correlated nuclear systems, the energy per nucleon of pure neutron matter as a function of the density contains relevant information for the behavior of nuclear systems beyond its isospin-symmetric state. In the BHF approximation, the energy per nucleon is given by the sum of a free kinetic term and the corresponding contribution of the sp spectrum,

$$\frac{B_{2N}}{A} = \frac{3}{10} \frac{k_F^2}{m} + \frac{1}{2} \frac{3}{k_F^3} \int_0^{k_F} k^2 dk U(k). \quad (20)$$

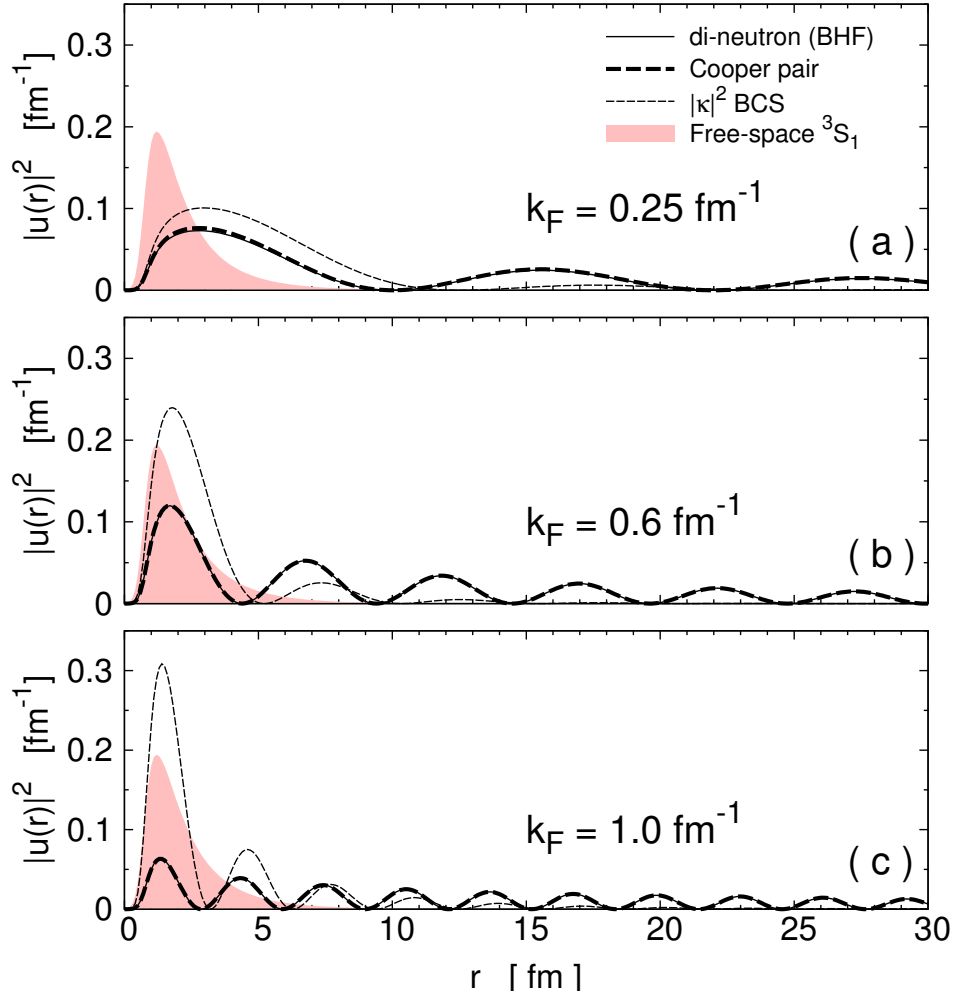


FIG. 8. Radial probability density for di-neutrons in  $^1S_0$  channel obtained from BHF equation (solid curves), Cooper-pair wave equation (long-dashed curves) and BCS anomalous density (short-dashed curves). Red-shaded curves in all frames represent the  $^3S_1$ -channel deuteron radial probability density in free space. Panels (a)-(c) correspond to solutions for  $k_F = 0.25, 0.60$ , and  $1.0 \text{ fm}^{-1}$ , respectively.

This expression is valid when Hamiltonians including 2NF only are used. When 3NF are included in the BHF calculations, these enter the calculations in two ways. First, a density-dependent two-body interaction is added to the bare 2NF in a standard  $G$ -matrix calculation. In addition, the total energy has to be corrected to avoid a double counting of the 3NF contribution [32, 46]. At the lowest order, this can be achieved by subtracting the

Hartree–Fock contribution due to 3NFs only:

$$\frac{B_{3N}}{A} = \frac{B_{2N}}{A} - \frac{1}{12} \frac{3}{k_F^3} \int_0^{k_F} k^2 dk \Sigma_{HF}^{3NF}(k). \quad (21)$$

We stress that the Hartree–Fock self–energy  $\Sigma_{HF}^{3NF}$  coming from the 3N force is calculated from the effective 2N potential at the lowest order, in keeping with the procedure established in the literature [32].

We show the calculated energy per neutron as a function of density in Fig. 9. Again, we show results based on AV18, Paris, N3LO<sub>2N</sub> and N3LO<sub>2N</sub>+N2LO<sub>3N</sub> bare interactions, corresponding to short–dashed, dash–dotted, dashed and solid curves, respectively. For all four cases, we find the well known monotonic growth of  $B/A$  with density. As expected, the case with chiral 3NFs provides the steepest increase in energy, with  $B/A \sim 50$  MeV at  $\rho = 0.4 \text{ fm}^{-3}$ . In contrast, the shallowest behavior is found for N3LO<sub>2N</sub>, a very soft nuclear interaction. We note, in particular, that its relatively low cutoff would normally preclude its use in densities well above saturation. The other two interactions (AV18 and Paris) lay in between these two chiral interactions. They provide very similar results in neutron matter, as expected from their quantitatively similar saturation points and symmetry energies within the BHF approximation [47].

The contribution of di–neutrons to the total energy is difficult to compute in this approach, but we expect it to be relatively small. First, the bound states enter the BHF calculations in a nonlinear way, through the  $G$ –matrix evaluation, and thus their contribution is included, in a sense, in the energy per particle of Eq. (20). Second, loosely bound di–neutrons appear in a narrow density regime, below  $\rho = 0.034 \text{ fm}^{-3}$ . In this region, the energy of homogeneous matter is substantially larger and hence dominates the total contribution. Third, an estimate of the contribution of di–neutrons to the total energy would require a calculation of the di–neutron concentration in neutron matter [8], an issue that goes beyond our preliminary analysis.

The results shown in Fig. 9 can be summarized with the following functional

$$\frac{B}{A} = \frac{K}{A} + a \left( \frac{\rho}{\rho_0} \right)^\alpha + b \left( \frac{\rho}{\rho_0} \right)^\beta, \quad (22)$$

where  $\rho_0 = 0.17 \text{ fm}^{-3}$  is the empirical saturation density of symmetric nuclear matter. We have separated explicitly the kinetic contribution,  $K/A = 3k_F^2/20m$ , from the potential terms. Coefficients of this parametrization are shown in II.

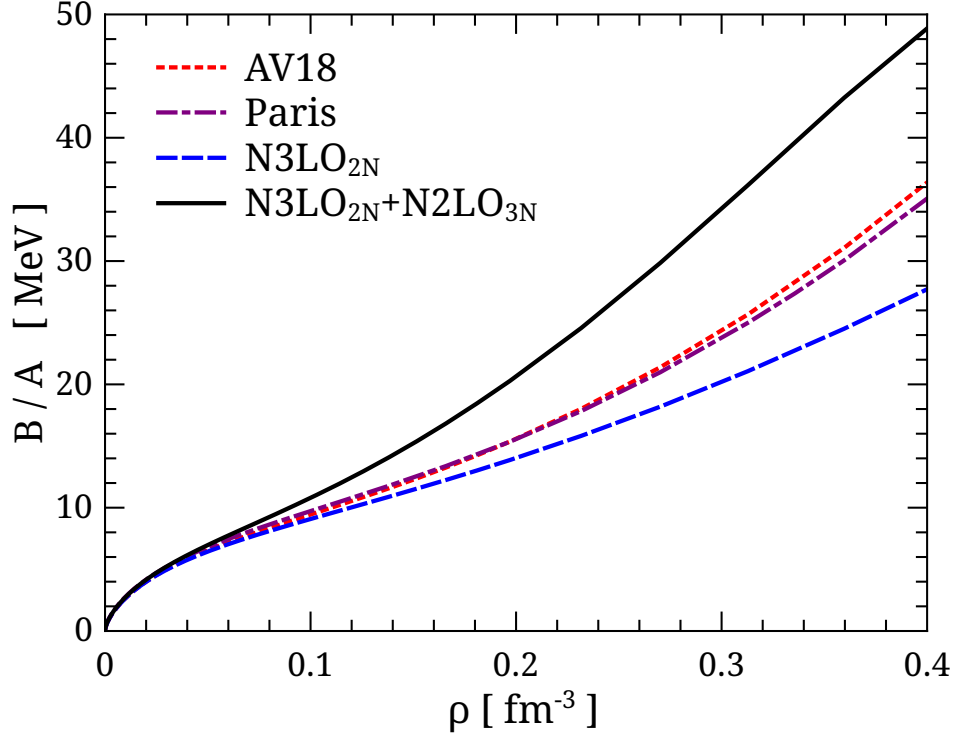


FIG. 9. Binding energy per neutron for pure neutronic matter as a function of density. Short-dashed, dash-dotted, dashed and solid curves correspond to AV18, Paris,  $N3LO_{2N}$  and  $N3LO_{2N}+N2LO_{3N}$  bare potentials, respectively.

	a	b	$\alpha$	$\beta$
	( MeV ) ( MeV )			
AV18	5.6520	-28.701	1.97	0.83
Paris	5.7215	-28.727	1.97	0.87
$N3LO_{2N}$	98.155	-122.14	1.13	1.03
$N3LO_{2N}+N2LO_{3N}$	17.767	-36.815	1.50	0.90

TABLE II. Fit coefficients for the energy per neutron,  $B/A$ , following Eq. (22).

#### IV. SUMMARY AND CONCLUSION

Within the BHF approach for pure neutron matter at zero temperature, we have investigated di-neutron structures with emphasis placed on the low-density regime. We have calculated self-consistent sp potentials at Fermi momenta up to  $2-3 \text{ fm}^{-1}$  using the continuous choice, restricting the system to a normal (nonsuperfluid) state. We have used AV18 and

Paris internucleon potential, in addition to chiral  $N^3LO_{2N}$  2NF as well as  $N^3LO_{2N}+N^2LO_{3N}$  3NF. Explicit account for di-neutron bound states is made in the  $^1S_0$  channel for the evaluation of the mass operator during self-consistent searches of the  $sp$  potential.

The resulting  $sp$  solutions from each of the potentials considered in this work are in fair agreement with those found elsewhere [27, 33, 47–49]. The major conclusion of our work is that di-neutron bound states appear in the BHF approach in the  $^1S_0$  channel independently of the Hamiltonian that is used to model neutron interactions. In terms of the Fermi momentum, di-neutrons appear in the regime  $0.06 \lesssim k_F \lesssim 1.05 \text{ fm}^{-1}$  and are loosely bound, by less than 700 keV. The density dependence of their binding energy is very close for all interactions, which indicates a dominance of many-body correlations in di-neutron formation. In particular, because they appear at low densities, di-neutrons do not seem to be affected by 3NF. More indicative, these bound states form at densities where neutron effective masses become larger than the bare mass. Furthermore, the size of these bound states can get as high as  $\sim 100 \text{ fm}$ . In contrast to isospin-symmetric nuclear matter, solutions for the  $sp$  spectra do not exhibit coexisting phases [12], mainly due to the fact that  $^3SD_1$  channel is fully suppressed in pure neutron matter. A recent study [50] addressing neutronic and symmetric nuclear matter, considering modern realistic  $NN$  interactions, confirms the robustness of these findings.

The study of nuclear matter, even on its simplest nonrelativistic form, is an exceedingly difficult problem involving various scenarios in density, isospin asymmetry and temperature. On top of that, the emergence of superfluidity, superconductivity and clusterization multiply the physical scenarios under which matter can evolve when confined. The study we have presented is just a first step towards *ab initio* clusterization studies, going beyond traditional calculations in this context which are based on a variety of phenomenological approximations. In turn, these calculations can provide guidance on clustering in isospin-rich systems.

We can foresee a variety of extension of this work, both at the phenomenological and at the more theoretical level. Within this very same framework, we would like to study the melting of di-neutrons as temperature effects switch on. The extension to isospin asymmetric systems is of relevance for neutron-star matter, but also in the context of nuclear structure and the isospin dependence of clustering correlations. The competition between pairing and bound states in neutron matter is relevant for BEC-BCS studies, and the BHF approach is perfectly suited to provide quantitative guidance on this subject. Finally, it would be

interesting to use other many-body techniques to establish firmly the existence of di-neutron bound states in isospin-rich nuclear systems.

## ACKNOWLEDGMENTS

H.F.A. acknowledges partial funding from FONDECYT under grant No 1120396. F.I. thanks funding from CONICYT under contract No. 221320081. This work was supported in part by STFC through Grants ST/I005528/1, ST/J000051/1 and ST/L005816/1. Partial support comes from “NewCompStar”, COST Action MP1304. F.I. thanks the hospitality of colleagues of the University of Surrey, UK, where part of this work took place.

- 
- [1] F. Kobayashi and Y. Kanada-En’yo, *Phys. Rev. C* **88**, 034321 (2013).
  - [2] A. Spyrou, Z. Kohley, T. Baumann, D. Bazin, B. A. Brown, G. Christian, P. A. DeYoung, J. E. Finck, N. Frank, E. Lunderberg, S. Mosby, W. A. Peters, A. Schiller, J. K. Smith, J. Snyder, M. J. Strongman, M. Thoennessen, and A. Volya, *Phys. Rev. Lett.* **108**, 102501 (2012).
  - [3] Y. Kanada-En’yo, Y. Taniguchi, and M. Kimura, *Journal of Physics: Conference Series* **111**, 012002 (2008).
  - [4] H.-W. Hammer and S. König, *Phys. Lett. B* **736**, 208 (2014).
  - [5] K. Kisamori, S. Shimoura, H. Miya, S. Michimasa, S. Ota, M. Assie, H. Baba, T. Baba, D. Beaumel, M. Dozono, T. Fujii, N. Fukuda, S. Go, F. Hammache, E. Ideguchi, N. Inabe, M. Itoh, D. Kameda, S. Kawase, T. Kawabata, M. Kobayashi, Y. Kondo, T. Kubo, Y. Kubota, M. Kurata-Nishimura, C. S. Lee, Y. Maeda, H. Matsubara, K. Miki, T. Nishi, S. Noji, S. Sakaguchi, H. Sakai, Y. Sasamoto, M. Sasano, H. Sato, Y. Shimizu, A. Stolz, H. Suzuki, M. Takaki, H. Takeda, S. Takeuchi, A. Tamii, L. Tang, H. Tokieda, M. Tsumura, T. Uesaka, K. Yako, Y. Yanagisawa, R. Yokoyama, and K. Yoshida, *Phys. Rev. Lett.* **116**, 052501 (2016).
  - [6] S. C. Pieper, *Phys. Rev. Lett.* **90**, 252501 (2003).
  - [7] A. Migdal, *Yadern. Fiz.* **16**, 427 (1972).
  - [8] M. Schmidt, G. Röpke, and H. Schulz, *Ann. Phys.* **202**, 57 (1990).
  - [9] S. Typel, G. Röpke, T. Klähn, D. Blaschke, and H. H. Wolter, *Phys. Rev. C* **81**, 015803 (2010).



- [10] R. A. Broglia and V. Zelevinsky, eds., *Fifty Years of Nuclear BCS* (World Scientific, Singapore, 2013).
- [11] G. Röpke, Phys. Rev. C **92**, 054001 (2015).
- [12] H. F. Arellano and J.-P. Delaroche, Eur. Phys. J. A **51**, 7 (2015).
- [13] S. Gandolfi, A. Gezerlis, and J. Carlson, Annual Review of Nuclear and Particle Science **65**, 303 (2015).
- [14] S. L. Shapiro and S. A. Teukolsky, *Black Holes, White Dwarfs, and Neutron Stars* (Wiley, Weinheim, 1983).
- [15] M. Hempel, J. Schaffner-Bielich, S. Typel, and G. Röpke, Phys. Rev. C **84**, 055804 (2011).
- [16] G. Shen, C. J. Horowitz, and E. O'Connor, Phys. Rev. C **83**, 065808 (2011).
- [17] W. Zwerger, ed., *The BCS-BEC crossover and the unitary Fermi gas*, Vol. 836 (Springer Science & Business Media, Berlin, 2011).
- [18] T. Alm, B. Friman, G. Röpke, and H. Schulz, Nucl. Phys. A **551**, 45 (1993).
- [19] J. Margueron, H. Sagawa, and K. Hagino, Phys. Rev. C **76**, 064316 (2007).
- [20] M. Jin, M. Urban, and P. Schuck, Phys. Rev. C **82**, 024911 (2010).
- [21] M. Stein, A. Sedrakian, X.-G. Huang, and J. W. Clark, Phys. Rev. C **90**, 065804 (2014).
- [22] J. W. Clark, A. Sedrakian, M. Stein, X.-G. Huang, V. A. Khodel, V. R. Shaginyan, and M. V. Zverev, J. Phys. Conf. Ser. **702**, 012012 (2016).
- [23] M. Stein, A. Sedrakian, X.-G. Huang, and J. W. Clark, Phys. Rev. C **93**, 015802 (2016).
- [24] V. A. Khodel, J. W. Clark, V. R. Shaginyan, and M. V. Zverev, Physics of Atomic Nuclei **77**, 1145 (2014).
- [25] W. H. Dickhoff and D. Van Neck, *Many-Body Theory Exposed* (World Scientific, Singapore, 2008).
- [26] H. Q. Song, M. Baldo, G. Giansiracusa, and U. Lombardo, Phys. Rev. Lett. **81**, 1584 (1998).
- [27] M. Baldo, A. Polls, A. Rios, H.-J. Schulze, and I. Vidaña, Phys. Rev. C **86**, 064001 (2012).
- [28] R. B. Wiringa, V. G. J. Stoks, and R. Schiavilla, Phys. Rev. C **51**, 38 (1995).
- [29] M. Lacombe, B. Loiseau, J. M. Richard, R. V. Mau, J. Côté, P. Pirès, and R. de Tourreil, Phys. Rev. C **21**, 861 (1980).
- [30] D. R. Entem and R. Machleidt, Phys. Rev. C **68**, 041001 (2003).
- [31] J. W. Holt, N. Kaiser, and W. Weise, Phys. Rev. C **81**, 024002 (2010).
- [32] K. Hebeler and A. Schwenk, Phys. Rev. C **82**, 014314 (2010).

- [33] A. Carbone, A. Rios, and A. Polls, Phys. Rev. C **90**, 054322 (2014).
- [34] A. Nogga, P. Navrátil, B. R. Barrett, and J. P. Vary, Phys. Rev. C **73**, 064002 (2006).
- [35] H. F. Arellano, *omp-online website* (2006 (accessed August 7, 2016)),  $U(k; k_F)$  solutions accessible for download from <http://www.omp-online.cl>.
- [36] N. Chamel, Phys. Rev. Lett. **110**, 011101 (2013).
- [37] M. Baldo, G. F. Burgio, H.-J. Schulze, and G. Taranto, Phys. Rev. C **89**, 048801 (2014).
- [38] N. Chamel, Nuclear Physics A **773**, 263 (2006).
- [39] H. Witała and W. Glöckle, Phys. Rev. C **85**, 064003 (2012).
- [40] A. Sedrakian and J. W. Clark, Phys. Rev. C **73**, 035803 (2006).
- [41] G. Röpke, A. Schnell, P. Schuck, and P. Nozières, Phys. Rev. Lett. **80**, 3177 (1998).
- [42] M. Baldo, U. Lombardo, and P. Schuck, Phys. Rev. C **52**, 975 (1995).
- [43] M. Matsuo, Phys. Rev. C **73**, 044309 (2006).
- [44] L. N. Cooper, Phys. Rev. **104**, 1189 (1956).
- [45] M. Baldo, J. Cugnon, A. Lejeune, and U. Lombardo, Nuclear Physics A **515**, 409 (1990).
- [46] A. Carbone, A. Polls, and A. Rios, Phys. Rev. C **88**, 044302 (2013).
- [47] Z. H. Li, U. Lombardo, H.-J. Schulze, W. Zuo, L. W. Chen, and H. R. Ma, Phys. Rev. C **74**, 047304 (2006).
- [48] K. Hebeler, J. M. Lattimer, C. J. Pethick, and A. Schwenk, Phys. Rev. Lett. **105**, 161102 (2010).
- [49] M. Baldo, G. F. Burgio, and I. Bombaci, Astron. Astrophys. **328**, 274 (1997).
- [50] H. F. Arellano, F. Isaule, and A. Rios, Eur. Phys. J. A **52**, 299 (2016).